Excitation Cross Sections of the $(n, n' \gamma)$ Reactions on Fe, Co, Ni, Cu, Zn, Mo, Ag, Cd and Sn

July 1965

日本原子力研究所
Japan Atomic Energy Research Institute

日本原子力研究所は、研究成果、調査結果の報告のため、つぎの3種の刊行物を、それぞれの通しナンバーを付して、不定期に発行しております.

1. 研究報告	まとまった研究の成果あるいはその一部における重要な結果の報告	JAERI 1001-3999
2. 調査報告	総説，展望，紹介などを含め，研究の成果，調査の結果をまとめたもの	JAERI 4001-5999
3. 資　　料	研究成果の普及，開発状況の紹介，施設共同利用の手引など	JAERI 6001-6999

このうち既刊分については「JAERI レポート一覧」にタイトル・要旨をまとめて掲載し、また新刊レポートは雑誌『原研』でその都度紹介しています. これらの刊行物に関する版権，複写のお問合せは，日本原子力研究所技術情報部あてお申し越しください.

なお、上記3種の報告は，日本原子力研究所生活協同組合（茨城県那珂郡東海村）で実費頒布をいたしております.

Japan Atomic Energy Research Institute publishes the nonperiodical reports with the following classification numbers.

1. **JAERI** 1001-3999 Research Reports.
2. **JAERI** 4001-5999 Survey Reports and Reviews.
3. **JAERI** 6001-6999 Information and Guiding Booklets.

Inquiries about these reports should be addressed to: Division of Technical Information. Japan Atomic Energy Research Institute, Tokai-mura, Naka-gun, Ibaraki-ken, Japan.

編集兼発行　日本原子力研究所　東京都港区芝田村町1の1 (電)591-5481

JAERI 1078 UDC 539.17.012 : 53.08

Excitation Cross Sections of the $(n, n'\gamma)$ Reactions on Fe, Co, Ni, Cu, Zn, Mo, Ag, Cd, and Sn

Summary

Excitation cross sections of $(n,n'\gamma)$ reactions have been measured on the low-lying levels of nuclei of mass number around 60 and 100, by using a ring-geometry arrangement for gamma-ray detection. Numerical values of the cross sections obtained for Fe, Co, Ni, Cu, Zn, Mo, Ag, Cd, and Sn are tabulated. Correction factors for finite angular resolution of the detecting system are calculated and listed. The equations used in calculating theoretical $(n,n'\gamma)$ cross sections are explicitly presented, and the calculated excitation curves and angular distributions of gamma rays are illustrated.

January 1965

Shiroh Kikuchi
Kotoyuki Okano
Kazuaki Nishimura
Division of Physics, Tokai Research Establishment
Japan Atomic Energy Research Institute

$(n, n'\gamma)$ 反応の励起断面積

要　　旨

質量数 60 および 100 あたりの核について，それらの低いエネルギー準位を励起する $(n, n'\gamma)$ 反応の励起曲線をリング・ジォメトリー法によって測定した．Fe, Co, Ni, Cu, Zn, Mo, Ag, Cd, および Sn について得られた断面積の値を表にして記した．90° における正確な微分断面積を算出するために必要な検出系の角分解能の補正を計算し，補正係数を表に示した．また $(n, n'\gamma)$ 反応断面積の理論値の計算に使用された具体的な式について述べ，2，3の場合について断面積やγ線の角度分布の計算結果を例示した．

1965 年 1 月

日本原子力研究所
東海研究所，物理部原子核物理研究室
菊　池　士　郎
岡　野　事　行
西　村　和　明

Contents

目　　次

1. Introduction

In an energy region below ~4 MeV, neutron induced reactions occur mainly through compound nucleus formation, and inelastic scattering cross sections of neutrons have generally been estimated by the statistical theory of nuclear reactions as proposed by HAUSER and FESHBACH[1]. Recently MOLDAUER proposed a modification to the Hauser-Feshbach formalism[2),3)].

According to these theories, the compound-nucleus formation cross section and the probability of its decay into a particular channel are related to the transmission coefficients of neutrons through the potential of a nucleus. The transmission coefficients can be determined by assuming an appropriate optical model potential for the interaction between incoming neutron and nucleus. The neutron inelastic scattering cross sections depend sensitively on the optical model parameters, especially on the value of the imaginary potential W.

As one of the methods of getting information on the optical model parameters, we have measured excitation cross sections of $(n, n'\gamma)$ reactions on the low-lying levels of Fe, Co, Ni, Cu, Zn, Mo, Ag, Cd, and Sn. Gamma rays were detected using a ring-geometry arrangement. The details of the experimental method and procedure, together with the discussions about the experimental results and theoretical predictions, are given in another publication[4)] to which this report is available as a supplement. In the next section, the numerical results obtained are presented. In section 3, the correction factors for finite angular resolution of the detecting system, which were used in ref. 4 for the evaluation of the experimental differential cross sections at 90°, are derived. The resultant values of the correction factors are tabulated in TABLE 5. The procedure of calculating the theoretical $(n, n'\gamma)$ differential cross sections based on a generalized Hauser-Feshbach formula[5)] is described in section 4.

2. Experimental Results

The $(n, n'\gamma)$ cross sections obtained at each neutron energy are listed in TABLES 1–4. The cross sections listed without parentheses were deduced by using the usual relation

$$\sigma_{\text{obs.}} = Y/\Phi N \varepsilon K, \qquad (1)$$

where Y is the gamma-ray counts under the photopeak produced, Φ is the neutron flux incident on a ring sample, N is the total number of relevant isotope in the sample, ε is the photopeak efficiency of the detector in the ring geometry, and K is the absorption correction of gamma rays in the sample material.

The cross sections thus obtained are nearly equal to 4π times the differential cross sections at 90°. The values of $4\pi(d\sigma(n,n'\gamma)/d\Omega_\gamma)_{\theta=90°}$ obtained after correcting for finite angular resolution of the detecting system are listed in parentheses in TABLES 1–4. The derivation of the correction factors is described in the next section.

3. Corrections for Finite Angular Resolution

Because of the finite sizes of the scatterer and of the NaI crystal used in the present experiment, the angles between the directions of the incident neutrons and those of the gamma rays detected range over several tens of degrees around 90°. For accurate evaluations of the differential cross sections at 90°, therefore, it is necessary to apply corrections for this effect to the cross sections obtained by eq. (1). The correction factor for this effect will be derived in the following. Gamma-ray counts Y can represented by

$$Y = \iiint \Phi e^{-\mu x} \frac{N}{V_1} d V_1 \sigma(\theta) d\Omega_\gamma e^{-\mu_1 x_1 - \mu_2 x_2} \rho_p dx_2, \qquad (2)$$

TABLE 1. Cross sections in millibarns for the $(n, n'\gamma)$ reactions on Fe, Co, and Ni. The isotopic cross sections are evaluated. The errors assigned are standard deviations. The values in parentheses are the cross sections corrected for finite angular resolution of the detecting system (see section 3). Cross sections for Fe designated by asterisks are the ones obtained by using granular iron as sample while others are those obtained by using a block iron.

E_n MeV	^{56}Fe E_γ=0.845MeV	^{59}Co E_γ=1.097 MeV	^{58}Co E_γ=1.189MeV	^{59}Co E_γ=1.289MeV	^{58}Ni E_γ=1.452 MeV	^{60,64}Ni $\bar{E}_\gamma$=1.33 MeV
1.001	285±20					
1.094		8±2				
1.148		28±6				
1.198		25±5	4±1			
1.219	330±23					
1.248		64±6	99±8			
1.298		44±4	96±7	1.4±0.5		25±12 (20)
1.347		41±5	103±8	10±3		
1.396		29±4	109±9	21±3	6±4 (5)	179±17 (145)
1.445		29±4	81±7	15±3		
1.494					48±5 (39)	281±24 (233)
1.596					157±12 (130)	341±33 (290)
1.698					278±21 (236)	306±43 (263)
1.799					382±28 (329)	232±52 (202)
1.897					355±26 (309)	300±50 (264)
1.999					377±28 (332)	436±58 (388)
2.022	775±53					
2.532	829±71					
"	866±75*					
2.558	885±76				476±43	651±83
"	899±77*					
2.584	800±69				460±41	679±84
"	823±71*					
2.610	733±63					
"	714±62*					
2.634	731±63					
"	739±64*					

TABLE 2. Cross sections in millibarns for the $(n, n'\gamma)$ reactions on Cu and Zn. The isotopic cross sections are evaluated. The errors assigned are standard deviations. The values in parentheses are the cross sections corrected for finite angular resolution of the detecting system (see section 3).

E_n MeV	^{63}Cu E_γ=0.668 MeV	^{63}Cu E_γ=0.961 MeV	^{65}Cu E_γ=0.770 MeV	^{65}Cu E_γ=1.114 MeV	Zn(even-even) $\bar{E}_\gamma$=1.02 MeV
0.633	4±3				
0.757	74±6		11±5		
0.788	84±7		13±5		
0.937	145±14	2±11	88±16		2±7 (2)
1.001	136±11	50±5	108±10		−6±7 (−5)
1.048					51±8 (42)
1.094	153±13	135±10	85±10	−0.6±0.1	128±11 (108)
1.148					172±14 (148)
1.198	161±14	214±15	87±11	112±11	224±17 (195)
1.248					281±20 (247)
1.298	164±15	274±19	97±13	132±12	317±23 (279)
1.347					362±25 (319)
1.396					382±27 (340)
1.445					415±29 (369)
1.494					440±31 (392)
1.546					446±31 (401)
1.596					479±33 (431)
1.646					531±37 (483)
1.698					558±39 (508)
1.746					598±41 (544)
1.799					595±41 (541)
2.558	191±27	551±49	194±68	584±56	885±61
2.584	203±27	550±48	230±75	569±56	854±59

TABLE 3. Cross sections in millibarns for the $(n, n'\gamma)$ reactions on Mo and Sn. The cross sections listed are the isotopic cross sections except those for 0.775-and 1.06-MeV gamma rays from Mo, where the atomic cross sections are evaluated. The errors assigned are standard deviations. The values in parentheses are the cross section corrected for finite angular resolution of the detecting system (see section 3).

E_n MeV	^{94}Mo E_γ=0.874 MeV		Mo $\bar{E}_\gamma$=0.775 MeV	Mo $\bar{E}_\gamma$=1.06 MeV	Sn(even-even) $\bar{E}_\gamma$=1.19 MeV	
0.788	−11± 15	(−10)	52± 7			
0.937	109±100	(102)	414±36			
1.001	381±113	(358)	414±35	0.5± 8		
1.094	1162±240	(1104)	477±40	−8±11	41±22	(34)
1.198	1550±304	(1473)	532±44	14± 5	113±24	(96)
1.248					82±21	(71)
1.298	1091±242	(1036)	594±50	77± 7	164±21	(143)
1.347					260±25	(229)
1.396	1099±240	(1044)	622±53	89± 8	296±27	(263)
1.445					338±28	(301)
1.494	1390±293	(1321)	596±52	67± 7	508±40	(457)
1.546					439±33	(399)
1.596					528±39	(480)
1.646					541±41	(492)
1.698					585±44	(532)
1.746					574±42	(522)
1.799					584±44	(531)
1.847					645±49	(593)
1.897					596±44	(548)
1.999					599±44	(551)

TABLE 4. Cross sections in millibarns for the $(n, n'\gamma)$ reactions on Ag and Cd. The cross sections for Ag are the isotopic cross sections while those for Cd are the atomic cross sections. The errors assigned are standard deviations. The values in parentheses are the cross sections corrected for finite angular resolution of the detecting system (see section 3). The cross-section values listed without associated errors are those obtained by normalizing the preliminary data to the present results, which were measured at four neutron energies. For Ag, the normalized preliminary data obtained by using the time-of-flight method are also listed without associated errors, to which the corrections for finite angular resolution of the detecting system are not applied. For the normalizations of the preliminary data to the present results, see ref. 4.

E_n MeV	^{107,109}Ag $\bar{E}_\gamma$=0.317 MeV		^{107,109}Ag $\bar{E}_\gamma$=0.420 MeV		Cd $\bar{E}_\gamma$=0.6 MeV	E_n MeV	^{107,109}Ag $\bar{E}_\gamma$=0.317 MeV		^{107,109}Ag $\bar{E}_\gamma$=0.420 MeV		Cd $\bar{E}_\gamma$=0.6 MeV
0.321	190	(188)				0.694	571	(565)	285	(271)	530
0.335	48					0.719	584	(578)	284	(270)	548
0.350	322	(318)				0.727	617±60	(611)	268±24	(254)	398±53
0.373	435	(430)				0.732	631		273		
0.394	330					0.743	519	(513)	244	(232)	484
0.398	429	(425)				0.757					521±70
0.423	464	(459)				0.769	650	(644)	325	(309)	496
0.448	462±45	(457)	66	(63)		0.784	601		300		
0.454	499		74			0.788					563±72
0.474	571	(565)	87	(83)		0.794	716	(708)	280	(266)	426
0.498	555	(549)	160	(152)		0.817	626	(620)	242	(230)	493
0.510	503		81			0.838	590		318		
0.520	682	(675)	157	(149)		0.843	623	(617)	251	(238)	513
0.545	707	(700)	166	(158)	82	0.869	626	(620)	202	(192)	565
0.567	567		168			0.891	606		309		
0.570	695	(688)	213	(202)	171	0.893	597	(591)	301	(286)	580
0.590	624±61	(618)	212±19	(202)		0.918	561	(555)	263	(250)	618
0.594	642	(635)	199	(189)	222	0.937	600±59	(594)	340±30	(323)	
0.619	608	(602)	234	(222)	339	0.942	553	(548)	291	(276)	619
0.623	589		234			0.944	624		347		
0.643	636	(630)	251	(238)	380	0.968	604	(598)	310	(294)	594
0.668	542	(536)	242	(230)	407	0.993	601	(595)	292	(278)	719
0.678			260								

where V_1 refers to the volume of the scatterer, $\sigma(\theta)$ is the differential cross section of the $(n, n'\gamma)$ reaction, Ω_γ is the solid angle into which the gamma rays are emitted. μ, μ_1, x, and x_1 are the neutron attenuation coefficient in the scatterer, the gamma-ray attenuation coefficient in the scatterer, the path length of the neutron in the scatterer, and the path length of the gamma ray in the scatterer, respectively. μ_2 and x_2 are the corresponding quantities for the gamma ray in the crystal. N and Φ represent the same quantities as those in eq. (1). μ_p is the effective photoabsorption coefficient for the gamma ray in the crystal. It refers not only to absorption by the photoelectric process but also to absorption by all multiple processes which produce a pulse in the full-energy peak[61].

Taking the cylindrical coordinate (ρ, φ, z) so that the z axis coincides with the cylindrical axis of the crystal,

$$\begin{aligned} dV_1 &= \rho_1 d\rho_1 d\varphi_1 dz_1 \\ dV_2 &= \rho_2 d\rho_2 d\varphi_2 dz_2 = r_{12}^2 d\Omega_\gamma dx_2 \\ r_{12}^2 &= \rho_1^2 + \rho_2^2 - 2\rho_1\rho_2\cos(\varphi_2-\varphi_1) + (z_2-z_1)^2, \end{aligned} \tag{3}$$

where, suffixes 1 and 2 refer to the scatterer and the crystal, respectively, and r_{12} is the distance between dV_1 and dV_2 as shown in Fig. 1. In the present investigation the gamma-

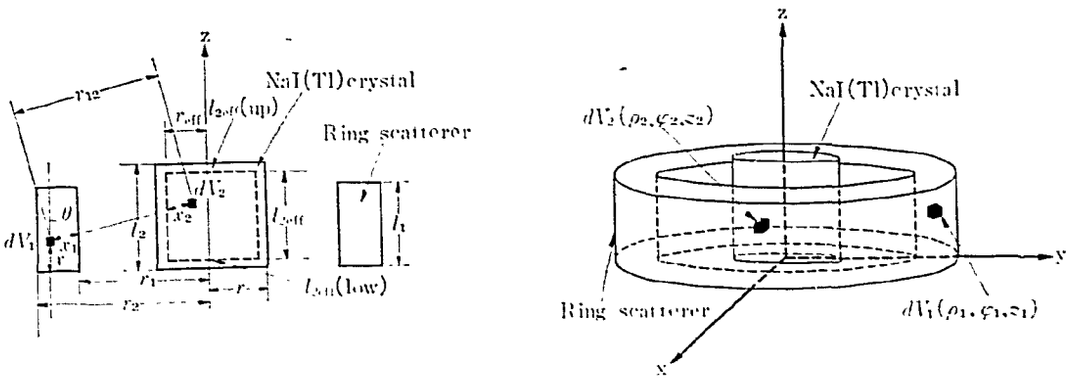

Fig. 1. Schematic diagram of the arrangement of the ring sample and NaI(Tl) crystal.

ray transitions are of E2 type, so that the differential cross section is represented by

$$\sigma(\theta) = a_0 + a_2\cos^2\theta + a_4\cos^4\theta. \tag{4}$$

Then,

$$\begin{aligned} Y = \int\cdots\int \Phi e^{-\mu x}\frac{N}{V_1}(a_0 + a_2\cos^2\theta + a_4\cos^4\theta)\, e^{-\mu_1 x_1 - \mu_2 x_2} \\ \times \mu_p \frac{\rho_1\rho_2 d\rho_1 d\rho_2 d\varphi_1 d\varphi_2 dz_1 dz_2}{\rho_1^2 + \rho_2^2 - 2\rho_1\rho_2\cos(\varphi_2-\varphi_1) + (z_2-z_1)^2}. \end{aligned} \tag{5}$$

For the gamma-ray energies now of interest, the effective photo-absorption coefficient μ_p is not a constant but depends on the direction of the incident gamma ray and on the position in the crystal where the incident gamma ray causes the first event. These facts make the direct evaluation of the integral difficult. However, the evaluation of the integral becomes easy, if one can find a certain effective volume V_2' of the crystal in such a way that

$$Y = \int_{V_1}\int_{V_2}\mu_p\cdots\cdots dV_1 dV_2 = \bar{\mu}_p\int_{V_1}\int_{V_2'}\cdots\cdots dV_1 dV_2'. \tag{6}$$

$\bar{\mu}_p$ is assumed to be constant in the effective volume V_2'.

Two additional assumptions are introduced. First, the effects of neutron multiple scattering cancel out neutron attenuation at the first collision[7], so that the factor $e^{-\mu x}$ in the integrand can be put equal to unity. Second, the incident neutron beam is parallel to the z axis throughout the scatterer, so that $\cos\theta$ is represented as

$$\cos\theta=\frac{z_2-z_1}{\sqrt{\rho_1^2+\rho_2^2-2\rho_1\rho_2\cos(\varphi_2-\varphi_1)+(z_2-z_1)^2}}. \tag{7}$$

In the case of the present investigation, it is estimated that about 20% of the incident neutrons undergo multiple scattering in the scatterer, and the directions of these neutrons differ from those of incident neutrons. In the present calculation, however, it is assumed that $\cos\theta$ is always given by eq. (7). Then, by using eqs. (5), (6), and (7),

$$Y=\frac{N}{V_1}\Phi\bar{\mu}_p(a_0I_0+a_2I_2+a_4I_4). \tag{8}$$

Here,

$$\begin{aligned}
I_0&=\int_{z_1=0}^{l_1}\int_{z_2=l_{2\mathrm{eff}}(low)}^{l_{2\mathrm{eff}}(up)}\int_{\varphi_1=0}^{2\pi}\int_{\varphi_2=0}^{2\pi}\int_{\rho_1=r_1}^{r_2}\int_{\rho_2=0}^{r_{\mathrm{eff}}} e^{-\mu_1x_1-\mu_2x_2}\\
&\quad\times\frac{\rho_1\rho_2d\rho_1d\rho_2d\varphi_1d\varphi_2dz_1dz_2}{\rho_1^2+\rho_2^2-2\rho_1\rho_2\cos(\varphi_2-\varphi_1)+(z_2-z_1)^2},\\
I_2&=\int\cdots\cdots\int e^{-\mu_1x_1-\mu_2x_2}(z_2-z_1)^2\,\frac{\rho_1\rho_2d\rho_1d\rho_2d\varphi_1d\varphi_2dz_1dz_2}{[\rho_1^2+\rho_2^2-2\rho_1\rho_2\cos(\varphi_2-\varphi_1)+(z_2-z_1)^2]^2},\\
I_4&=\int\cdots\cdots\int e^{-\mu_1x_2-\mu_2x_2}(z_2-z_1)^4\,\frac{\rho_1\rho_2d\rho_1d\rho_2d\varphi_1d\varphi_2dz_1dz_2}{[\rho_1^2+\rho_2^2-2\rho_1\rho_2\cos(\varphi_2-\varphi_1)+(z_2-z_1)^2]^3},
\end{aligned} \tag{9}$$

where r_1, r_2, and l_1 are the inner radius, the outer radius, and the axial thickness of the ring scatterer, respectively. r_{eff}, $l_{2\mathrm{eff}}(low)$, and $l_{2\mathrm{eff}}(up)$ are the radius, the lower end, and the upper end of the effective volume of the crystal, respectively, as shown in Fig. 1.

Now, the cross section averaged over the directions of gamma rays emitted is given by

$$\begin{aligned}
\langle\sigma(\theta)\rangle&=\frac{\iint\Phi\frac{N}{V_1}e^{-\mu_1x_1-\mu_2x_2}\sigma(\theta)\,\bar{\mu}_p\frac{1}{r_{12}^2}dV_1dV_2'}{\iint\Phi\frac{N}{V_1}e^{-\mu_1x_1-\mu_2x_2}\bar{\mu}_p\frac{1}{r_{12}^2}dV_1dV_2'}\\
&=\frac{Y}{\bar{\mu}_p\Phi\frac{N}{V_1}\iint e^{-\mu_1x_1-\mu_2x_2}\frac{1}{r_{12}^2}dV_1dV_2'}\\
&=\frac{a_0I_0+a_2I_2+a_4I_4}{I_0}.
\end{aligned} \tag{10}$$

The integral in the denominator in eq. (10) is connected with ε and K as

$$\frac{1}{4\pi V_1}\iint e^{-\mu_1x_1-\mu_2x_2}\,\bar{\mu}_p\frac{1}{r_{12}^2}dV_1dV_2'=\varepsilon K. \tag{11}$$

Thus, eq. (10) can be written as

$$\langle\sigma(\theta)\rangle=\frac{Y}{4\pi\Phi N\varepsilon K}=\frac{\sigma_{\mathrm{obs.}}}{4\pi}. \tag{12}$$

The correction factor K which reduces the cross sections experimentally obtained to precise 4π times the differential cross sections at 90° is, therefore

$$k = \frac{4\pi\sigma(90°)}{\sigma_{obs.}} = \frac{\sigma(90°)}{<\sigma(\theta)>} = \frac{a_0 I_0}{a_0 I_0 + a_2 I_2 + a_4 I_4}. \tag{13}$$

In order to obtain this correction factor numerically, it is necessary to estimate the effective radius and the effective length of the crystal. They were approximately obtained by the simple measurements as following. First, the crystal was irradiated by a collimated gamma-ray beam of 3-mm diameter parallel to the cylindrical axis, along a diameter of the front face with intervals of 2 mm. The gamma-ray counting rates were measured and the effective radius of the crystal was estimated by putting the integral of the gamma-ray counts over the diameter equal to $2r_{eff}$ times the gamma-ray counts obtained at the center of the diameter. Next, the crystal was irradiated by the gamma-ray beam perpendicular to the cylindrical axis. The effective length of the crystal was estimated by the same procedure as that for the effective radius. In both measurements, counting rates measured were constant in the inner region of the crystal while they decreased near the edge. The 0.511- and 1.274-MeV gamma rays from ^{22}Na were used for the measurements.

For the gamma rays from the $(n,n'\gamma)$ reactions studied, the effective radius and the effective length of the crystal were obtained by inter- or extrapolation of the measured values concerning the gamma-ray energy, which ranged from about 0.85 to 0.95 of the actual radius and length of the crystal depending upon the energy of incident gamma ray.

The uncertainty in the determination of the effective dimension of the crystal affects the correction factor very little. As an extreme case, for example, the correction factor for zinc calculated with a half of the actual radius and a half of the actual length of the crystal was larger by only 2% than that calculated with the effective dimension obtained by the method described above.

I_0, I_2, and I_4 were computed by the IBM 7044 computer*. For a_0, a_2, and a_4, theoretical values calculated by using the generalized Hauser-Feshbach formula[5] with Beyster's transmission coefficients[8] were adopted. The numerical values of the correction factors thus obtained for Ni, Zn, Mo, Ag, and Sn are tabulated in TABLE 5.

4. Theoretical Cross Sections

The $(n,n'\gamma)$ cross sections based on the Hauser-Feshbach theory have been calculated according to the following expression, which was derived by SUGIE[5] generalizing the Hauser-Feshbach equation :

$$\begin{aligned}
\frac{d\sigma(i,i';i'')}{d\Omega_\gamma} = {} & \frac{\lambda^2}{8(2i+1)} \sum_{L=\text{even}} \sum_{J\pi} \frac{(2J+1)}{\sum_{\text{fixed}J\pi} T_{i''j''}(E'')} (-1)^{i+i''} \\
& \times \sum_{lj} (2j+1)\,(jj1/2\ -1/2\,|\,L0)\ \sqrt{2J+1}\ W(jJjJ\,;\,i\,L)\ T_{ij}(E) \\
& \times \sum_{l'j'} (-1)^{j'-1/2}\ \sqrt{(2J+1)\,(2i'+1)}\ W(i'Ji'J\,;\,j'\,L)\ T_{i'j'}(E') \\
& \times \sum_{\substack{\Lambda P \\ \Lambda' P'}} \sqrt{(2\Lambda+1)\,(2\Lambda'+1)}\ (\Lambda\Lambda'1-1|\ L\,0)\ \sqrt{2i'+1}\ W(i'\Lambda\, i'\Lambda'\,;\,i''L) \\
& \times a_{\Lambda P}\, a_{\Lambda' P'}\, P_L(\cos\theta).
\end{aligned} \tag{14}$$

* Program CORARE

TABLE 5. Correction factors for finite angular resolution of the detecting system. The theoretical angular distributions of gamma rays calculated by using the generalized Hauser-Feshbach formula[5], with Beyster's transmission coefficients[6], are adopted for calculations. The correction factors for the 0.775-MeV line from molybdenum are used in section 5 of ref. 4, where the isotopic cross sections are shown for this line in order to compare the observed cross sections with the calculated ones by assuming that this line originates from ^{96}Mo and ^{98}Mo.

E_n MeV	^{58}Ni E_γ=1.452 MeV	^{60,64}Ni E_γ=1.33 MeV	Zn E_γ=1.02 MeV	^{94}Mo E_γ=0.874 MeV	^{96,98}Mo E_γ=0.775 MeV	Ag E_γ=0.317 MeV	Ag E_γ=0.420 MeV	Sn E_γ=1.19 MeV
0.40						0.99		
0.50						0.99	0.95	
0.60						0.99	0.95	
0.75						0.99	0.95	
0.90					0.95			
1.00				0.94	0.95			
1.10			0.84	0.95	0.95			
1.20				0.95	0.95			
1.30			0.88	0.95	0.95			0.87
1.40		0.81		0.95	0.95			
1.50	0.81	0.83	0.89	0.95	0.95			0.90
1.60	0.83	0.85						
1.70	0.85	0.86	0.91					0.91
1.80	0.86	0.87						
1.90	0.87	0.88	0.91					0.92
2.00	0.88	0.89						

Here $T_l^j(E)$ is the transmission coefficient for l-th partial wave with $\boldsymbol{j}=\boldsymbol{l}+\boldsymbol{s}$, and can be derived from optical model potentials. Other notations are : i, spin of the target ground state, i', spin of the excited state to which inelastic scattering occurs, i'', spin of the state to which gamma-ray decay leads, $J\pi$, spin and parity of the compound state, l, P, multipole order and parity of gamma ray, $a_{l'}^{P'}$ relative transition amplitude of gamma ray normalized to unity.

This equation reduces to a simpler form for the special case that the first excited state in the even-even nucleus is excited, followed by an E2 transition to the ground state :

$$\frac{d\sigma(0,2;0)}{d\Omega_\gamma}=\frac{\lambda^2}{8}\sum_{L=\text{even}}\sum_{J\pi}\sum_{\substack{lj\\l'j'}}(2j+1)\frac{T_l^j(E)\,T_{l'}^{j'}(E')}{\sum_{\text{fixed}J\pi}T_{l''}^{j''}(E'')}\,C^L(jj')P_L(\cos\theta), \tag{15}$$

where

$$C^L(jj')=(-1)^{j'+1/2}\,5(2j+1)\,(2\,2\,1-1|\,L\,0)\,(jj1/2-1/2|\,L\,0)\,W(2j2j';j'L). \tag{16}$$

If the contributions of partial waves with orbital angular momentum $l\geq 4$ or $l'\geq 4$ are neglected, the equation can be expressd as follows :

$$\frac{8}{\lambda^2}\frac{d\sigma(0,2;0)}{d\Omega_\gamma}=\left\{\frac{2T_0^{1/2}(E)\left[T_2^{3/2}(E')+T_2^{5/2}(E')\right]}{T_0^{1/2}(E)+T_2^{3/2}(E')+T_2^{5/2}(E')}\right.$$

$$+\frac{2T_1^{1/2}(E)\left[T_1^{3/2}(E')+T_3^{5/2}(E')\right]}{T_1^{1/2}(E)+T_1^{3/2}(E')+T_3^{5/2}(E')}$$

$$+\frac{4T_2^{3/2}(E)\left[T_0^{1/2}(E')+T_2^{3/2}(E')+T_2^{5/2}(E')\right]}{T_2^{3/2}(E)+T_0^{1/2}(E')+T_2^{3/2}(E')+T_2^{5/2}(E')}$$

$$+\frac{4T_1^{3/2}(E)\left[T_1^{1/2}(E')+T_1^{3/2}(E')+T_3^{5/2}(E')+T_3^{7/2}(E')\right]}{T_1^{3/2}(E)+T_1^{1/2}(E')+T_1^{3/2}(E')+T_3^{5/2}(E')+T_3^{7/2}(E')}$$

$$+\frac{6T_2^{5/2}(E)\left[T_0^{1/2}(E')+T_2^{3/2}(E')+T_2^{5/2}(E')\right]}{T_2^{5/2}(E)+T_0^{1/2}(E')+T_2^{3/2}(E')+T_2^{5/2}(E')}$$

$$+\frac{6T_3^{5/2}(E)\left[T_1^{1/2}(E')+T_1^{3/2}(E')+T_3^{5/2}(E')+T_3^{7/2}(E')\right]}{T_3^{5/2}(E)+T_1^{1/2}(E')+T_1^{3/2}(E')+T_3^{5/2}(E')+T_3^{7/2}(E')}$$

$$\left.+\frac{8T_3^{7/2}(E)\left[T_1^{3/2}(E')+T_3^{5/2}(E')+T_3^{7/2}(E')\right]}{T_3^{7/2}(E)+T_1^{3/2}(E')+T_3^{5/2}(E')+T_3^{7/2}(E')}\right\}P_0(\cos\theta)$$

$$+\left\{\frac{4T_2^{3/2}(E)\left[\frac{1}{2}T_0^{1/2}(E')-\frac{5}{14}T_2^{5/2}(E')\right]}{T_2^{3/2}(E)+T_0^{1/2}(E')+T_2^{3/2}(E')+T_2^{5/2}(E')}\right.$$

$$+\frac{4T_1^{3/2}(E)\left[\frac{1}{2}T_1^{1/2}(E')-\frac{5}{14}T_3^{5/2}(E')+\frac{1}{7}T_3^{7/2}(E')\right]}{T_1^{3/2}(E)+T_1^{1/2}(E')+T_1^{3/2}(E')+T_3^{5/2}(E')+T_3^{7/2}(E')}$$

$$+\frac{6T_2^{5/2}(E)\left[\frac{4}{7}T_0^{1/2}(E')+\frac{10}{49}T_2^{3/2}(E')-\frac{10}{49}T_2^{5/2}(E')\right]}{T_2^{5/2}(E)+T_0^{1/2}(E')+T_2^{3/2}(E')+T_2^{5/2}(E')}$$

$$+\frac{6T_3^{5/2}(E)\left[\frac{4}{7}T_1^{1/2}(E')+\frac{10}{49}T_1^{3/2}(E')-\frac{10}{49}T_3^{5/2}(E')-\frac{17}{49}T_3^{7/2}(E')\right]}{T_3^{5/2}(E)+T_1^{1/2}(E')+T_1^{3/2}(E')+T_3^{5/2}(E')+T_3^{7/2}(E')}$$

$$\left.+\frac{8T_3^{7/2}(E)\left[\frac{25}{49}T_1^{3/2}(E')+\frac{25}{294}T_3^{5/2}(E')-\frac{40}{147}T_3^{7/2}(E')\right]}{T_3^{7/2}(E)+T_1^{3/2}(E')+T_3^{5/2}(E')+T_3^{7/2}(E')}\right\}P_2(\cos\theta)$$

$$+\left\{\frac{6T_2^{5/2}(E)\left[-\frac{4}{7}T_0^{1/2}(E')+\frac{32}{49}T_2^{3/2}(E')-\frac{18}{49}T_2^{5/2}(E')\right]}{T_2^{5/2}(E)+T_0^{1/2}(E')+T_2^{3/2}(E')+T_2^{5/2}(E')}\right.$$

$$+\frac{6T_3^{5/2}(E)\left[-\frac{4}{7}T_1^{1/2}(E')+\frac{32}{49}T_1^{3/2}(E')-\frac{18}{49}T_3^{5/2}(E')+\frac{16}{147}T_3^{7/2}(E')\right]}{T_3^{5/2}(E)+T_1^{1/2}(E')+T_1^{3/2}(E')+T_3^{5/2}(E')+T_3^{7/2}(E')}$$

$$\left.+\frac{8T_3^{7/2}(E)\left[-\frac{18}{49}T_1^{3/2}(E')+\frac{32}{49}T_3^{5/2}(E')-\frac{24}{49}T_3^{7/2}(E')\right]}{T_3^{7/2}(E)+T_1^{3/2}(E')+T_3^{5/2}(E')+T_3^{7/2}(E')}\right\}P_4(\cos\theta). \tag{17}$$

Furthermore, if the optical potential does not include spin orbit force as in the case of Beyster or Emmerich potential, T_l^j is j independent, *i.e.*, $T_l^{l-1/2}=T_l^{l+1/2}=T_l$, so that

the above equation reduces to

$$\frac{4}{\chi^2}\frac{d\sigma}{d\Omega_\gamma}=\left\{\frac{2T_0(E)\,T_2(E')}{T_0(E)+2T_2(E')}+\frac{T_1(E)\,[T_1(E')+T_3(E')]}{T_1(E)+T_1(E')+T_3(E')}\right.$$
$$+\frac{5T_2(E)\,[T_0(E')+2T_2(E')]}{T_2(E)+T_0(E')+2T_2(E')}+\frac{4T_1(E)\,[T_1(E')+T_3(E')]}{T_1(E)+2T_1(E')+2T_3(E')}$$
$$\left.+\frac{6T_3(E)\,[T_1(E')+T_3(E')]}{T_3(E)+2T_1(E')+2T_3(E')}+\frac{4T_3(E)\,[T_1(E')+2T_3(E')]}{T_3(E)+T_1(E')+2T_3(E')}\right\}P_0(\cos\theta)$$
$$+\left\{\frac{T_2(E)\left[\frac{19}{7}T_0(E')-\frac{5}{7}T_2(E')\right]}{T_2(E)+T_0(E')+2T_2(E')}+\frac{T_1(E)\left[T_1(E')-\frac{3}{7}T_3(E')\right]}{T_1(E)+2T_1(E')+2T_3(E')}\right.$$
$$\left.+\frac{3T_3(E)\left[\frac{38}{49}T_1(E')-\frac{27}{49}T_3(E')\right]}{T_3(E)+2T_1(E')+2T_3(E')}+\frac{4T_3(E)\left[\frac{25}{49}T_1(E')-\frac{55}{294}T_3(E')\right]}{T_3(E)+T_1(E')+2T_3(E')}\right\}P_2(\cos\theta)$$
$$+\left\{\frac{6T_2(E)\left[-\frac{2}{7}T_0(E')+\frac{1}{7}T_2(E')\right]}{T_2(E)+T_0(E')+2T_2(E')}+\frac{6T_3(E)\left[\frac{2}{49}T_1(E')-\frac{19}{147}T_3(E')\right]}{T_3(E)+2T_1(E')+2T_3(E')}\right.$$
$$\left.+\frac{8T_3(E)\left[-\frac{9}{49}T_1(E')+\frac{4}{49}T_3(E')\right]}{T_3(E)+T_1(E')+2T_3(E')}\right\}P_4(\cos\theta). \qquad (18)^*$$

The $(n, n'\gamma)$ cross sections were calculated by using the transmission coefficients derived from the optical model potentials of Beyster *et al.*[8], Bjorklund and Fernbach[11], Perey and Buck[12], Emmerich[13], and Sugie[5]. The numerical values were taken from the published tables[8),13),14)] except for the Sugie potential, in which case the transmission coefficients were calculated by the IBM 7044 computer** for several depths of the imaginary potential W. For even-even nuclei such as Ni, Zn, Mo, and Sn, eq. (17) or (18) was applied. For odd-even nuclei Ag, more complicated equations derived from eq. (14) were used. In each case, numerical calculations were performed by the IBM computer***.

In Figs. 2 and 3, the excitation cross sections of the $(n, n'\gamma)$ reactions on Zn and Ag evaluated at $\theta=90°$ $(4\pi(d\sigma(n,n'\gamma)/d\Omega_\gamma)_{\theta=90°})$ are shown together with the experimental points. Similar curves for Ni, Mo, and Sn are presented in ref. 4. The inelastic cross sections integrated over angles are also plotted in Fig. 4. The angular distributions of gamma rays for Zn and Ag calculated by using several types of potentials are shown in Figs. 5 and 6. The curves shown are normalized so that the integrated cross sections over angles are equal.

From Figs. 2 and 3 it can be seen that the inelastic scattering cross sections are sensitive to the shape and parameters of the optical model potential adopted. The angular distributions of gamma rays are not so sensitive, however, as are seen from Figs. 5 and 6. The general trend that the experimental cross sections are smaller than the theoretically

---

* Satchler also derived a similar formula for the angular distributions of gamma rays following inelastic neutron scattering[9),10)]. A comparison of equation (18) with corresponding equation (last equation in ref. 10) shows that two errors are involved in Satchler's equation, *i.e.*, $P_2(\cos\theta)$ should be replaced by $[4+P_2(\cos\theta)]$ and $[10+0.714\ P_2(\cos\theta)+\cdots\cdots]$ should be read as $[10-0.714\ P_2(\cos\theta)+\cdots\cdots]$.

** Program NPOP

*** Program INNGE for even-even nucleus
INNGAG for Ag.

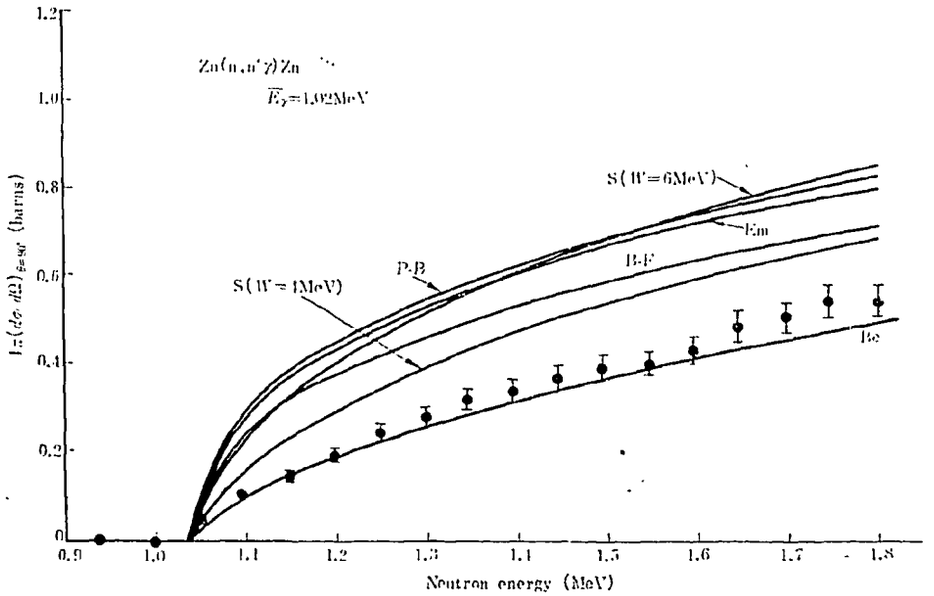

Fig. 2. Excitation cross sections of the Zn $(n,n'\gamma)$ reaction evaluated at $\theta=90°$ $(4\pi(d\sigma(n,n'\gamma)/d\Omega_\gamma)_{\theta=90°})$, using the transmission coefficients derived from several types of optical model potentials. The optical potential used is indicated on each curve by the initials of the authors who proposed the potential. The closed circles show the experimental cross sections corrected for finite angular resolution of the detecting system. In all the cases, the isotopic cross sections averaged over even isotopes of Zn are evaluated.

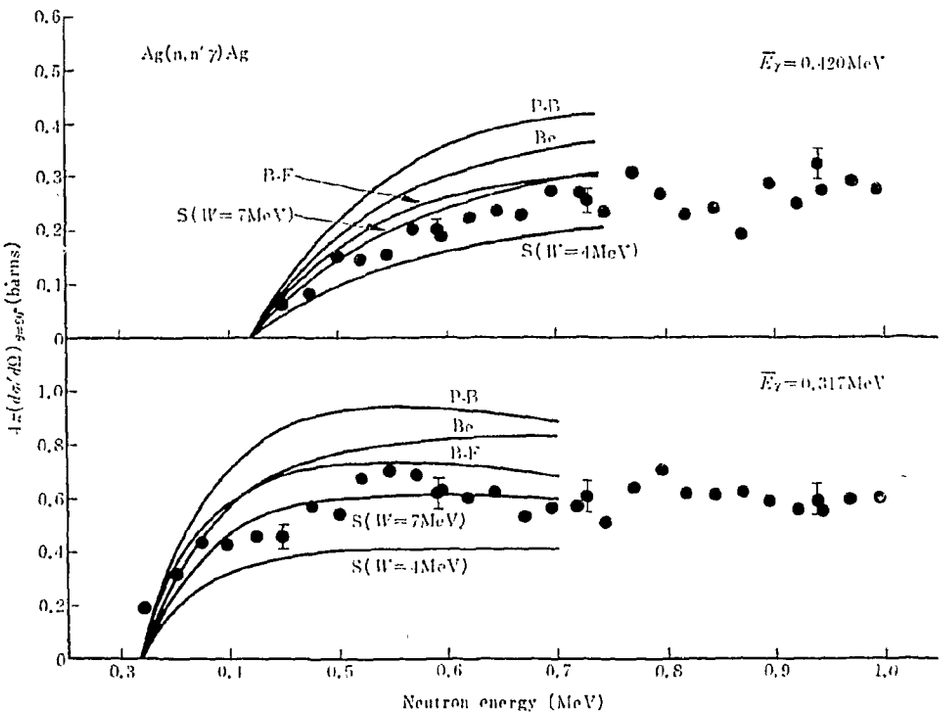

Fig. 3. Excitation cross sections of the Ag $(n,n'\gamma)$ reactions evaluated at $\theta=90°$ $(4\pi(d\sigma(n,n'\gamma)/d\Omega_\gamma)_{\theta=90°})$, using the transmission coefficients derived from optical model potentials. The optical potential used is indicated on each curve by the initials of the authors as is in Fig. 2. The closed circles show the experimental cross sections corrected for finite angular resolution of the detecting system.

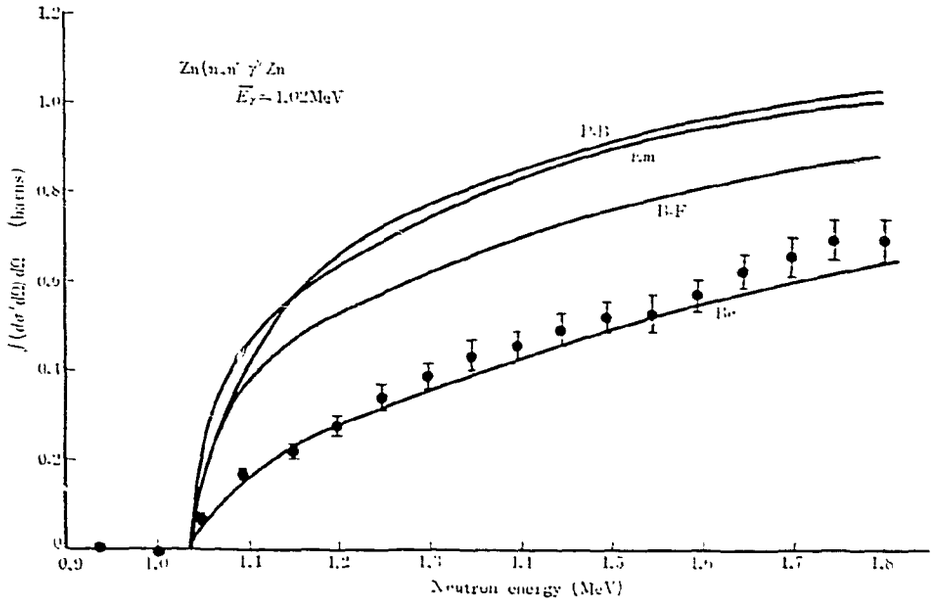

(a)

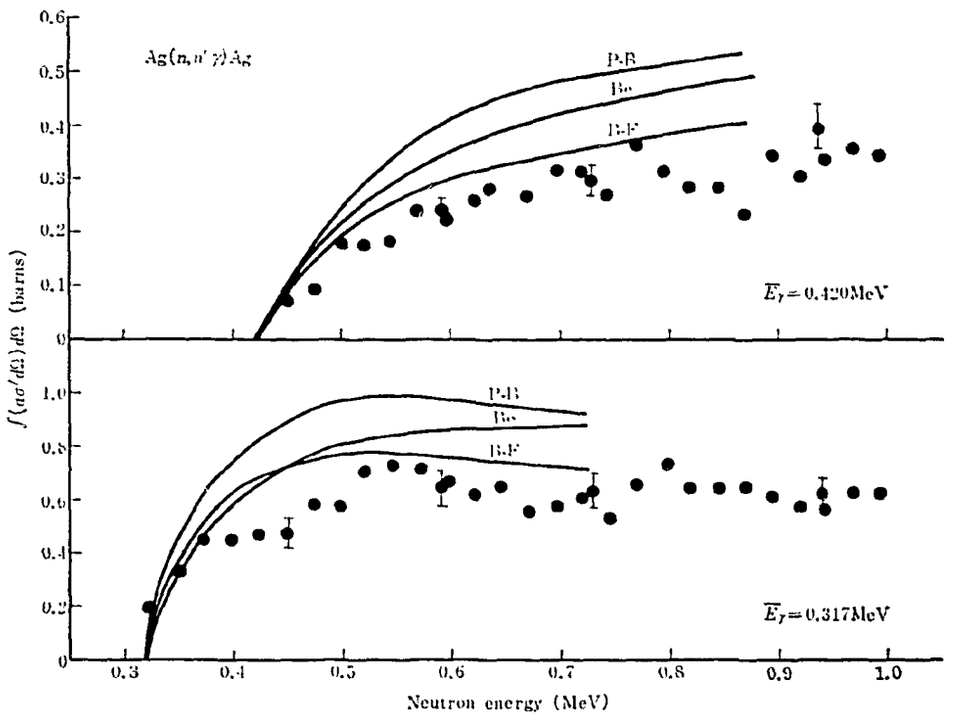

(b)

Fig. 4. Excitation cross sections of the $(n,n'\gamma)$ reactions on Zn and Ag integrated over angles. The experimental cross sections shown by circles were derived from the experimental differential cross sections obtained at θ=90°, assuming the theoretical angular distributions for the gamma ray.

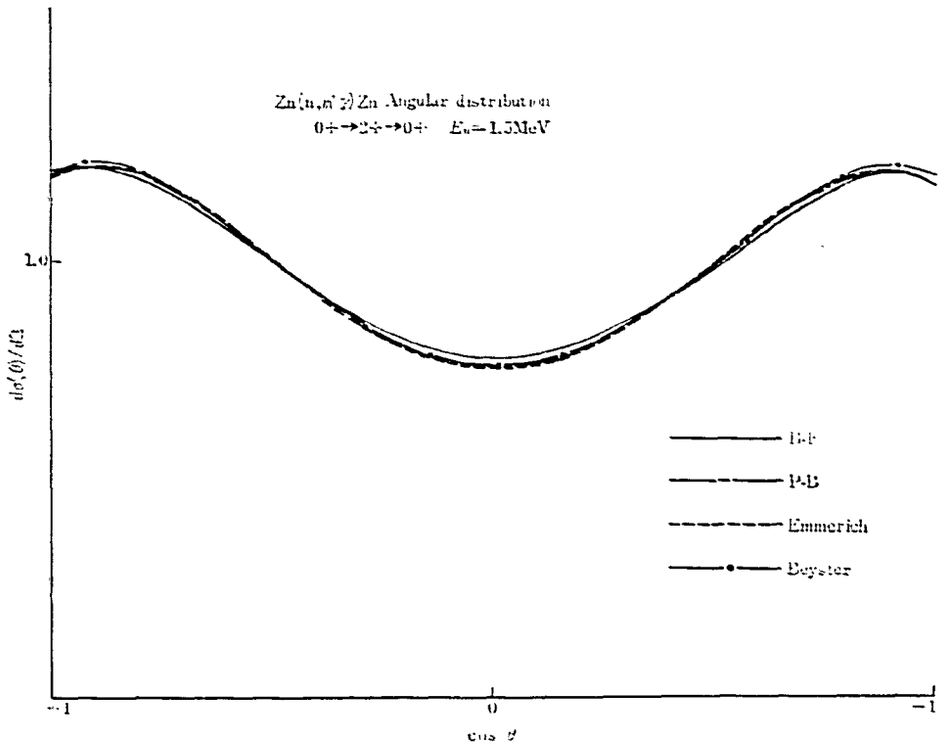

Fig. 5. Theoretical angular distributions of the 1.02-MeV gamma ray from the Zn $(n,n'\gamma)$ reaction, averaged over even isotopes. Angular distribution curves calculated from several types of optical model potentials are shown. These curves are normalized so that the integrated cross sections over angles are equal.

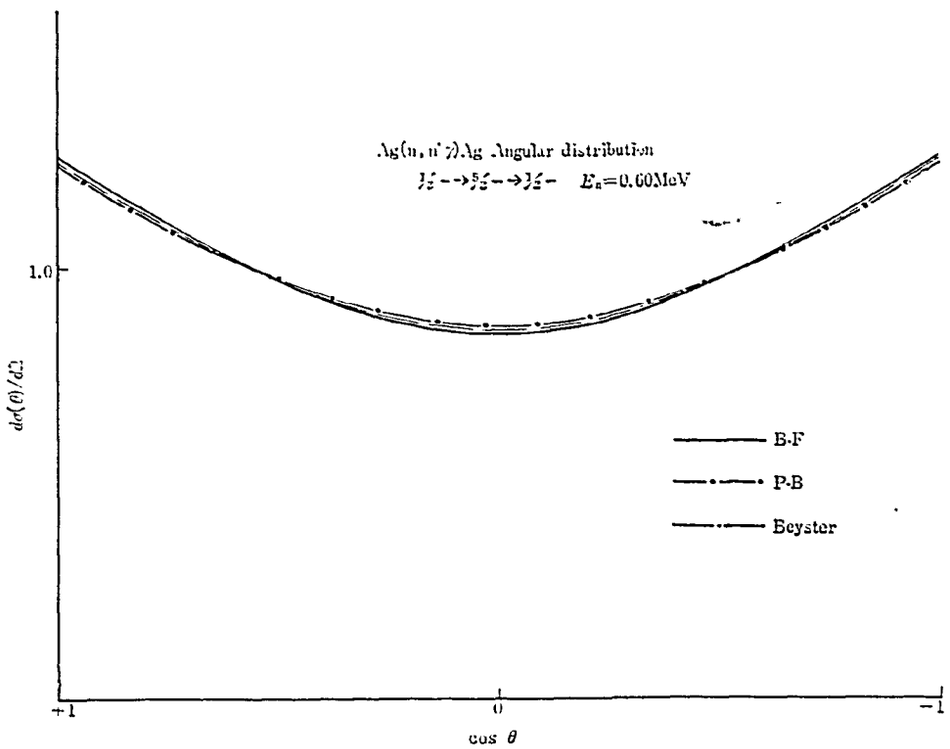

Fig 6. Theoretical angular distributions of the 0.420-MeV gamma ray from the Ag $(n,n'\gamma)$ reaction. Angular distribution curves calculated from several types of optical model potentials are shown. These curves are normalized so that the integrated cross sections over angles are equal.

calculated ones[4] seems to suggest that the value of the imaginary potential W is smaller at the neutron energy range of interest ($E_n \lesssim 2$ MeV). In this energy range, however, the number of competing outgoing channels is small, and the Hauser-Feshbach formalism may not have complete validity. The level width fluctuation effect[15],[16] tends to decrease the inelastic scattering cross sections. Recently Moldauer developed a revised theory[2],[3],[17] which includes the level width fluctuation effect as well as the revised relationship between optical model absorption and average compound nucleus formation. The inelastic scattering cross sections calculated by this theory are in general considerably smaller[17],[18],[19],[20] than those calculated by the Hauser-Feshbach theory. Fairly good agreement has been obtained[4] in the case of Zn between experimental cross sections and those calculated by the Moldauer theory using the transmission coefficients derived from Perey-Buck potential. These facts indicate that the ambiguities involved in the formulation of statistical theory itself affect seriously upon the cross sections in the neutron energy range considered here. The development of a theoretical formalism based on firmer ground is earnestly desirable.

Acknowledgments

We would like to express our sincere thanks to Dr. T. Momota, Dr. K. Tsukada, and other members of the Van de Graaff group for their interests and encouragements. We are much indebted to Dr. A. Sugie for his contributions to the theoretical analysis concerning the present work and for his illuminating suggestions and discussions. We are also indebted to Messrs. M. Akanuma, S. Momiyama, T. Tsutsui, and N. Saito for programing and executing the numerical calculations. Thanks are also due to Messrs. Y. Sato and T. Yoshida for their helpful assistances.

References

1) W. Hauser and H. Feshbach : *Phys. Rev.*, **87**, 366 (1952)
2) P. A. Moldauer : *Phys. Rev.*, **123**, 968 (1961)
3) P. A. Moldauer : *Phys. Rev.*, **129**, 754 (1963)
4) K. Nishimura, K. Okano, and S. Kikuchi : to be published
5) A. Sugie, S. Kikuchi, S. Momiyama, and T. Suzuki : *Progr. Theoret. Phys.*, (Kyoto),**26**, 797 (1961) ; *ibid.*, **27**, 422 (1962)
6) W. E. Mott and R. B. Sutton : "Encyclopedia of Physics", Springer-Verlag, Berlin, **45**, 86 (1958), edited by S. Flügge
7) R. B. Day : *Phys. Rev.*, **102**, 767 (1957)
8) J. R. Beyster, R. G. Schrandt, M. Walt, and E. Salmi : Los Alamos Scientific Laboratory Report, LA-2099 (1957) (unpublished)
9) G. R. Satchler : *Phys. Rev.*, **94**, 1304 (1954)
10) G. R. Satchler : *Phys. Rev.*, **104**, 1198Å (1956)
11) F. Bjorklund and S. Fernbach : *Phys. Rev.*, **109**, 1295 (1958)
12) F. Perey and B. Buck : *Nuclear Phys.*, **32**, 353 (1962)
13) W. S. Emmerich : Westinghouse Research Report 6-94511-6-R19 (1958) (unpublished)
14) E. H. Auerbach and F. G. J, Perey : Brookhaven National Laboratory Report, BNL-765 (T-286) (1962) (unpublished)
15) A. M. Lane and J. E. Lynn : *Proc. Phys. Soc.*, (*London*), **A70**, 557 (1957)
16) I. Dresner : Proceedings of the International Conference on Neutron Interactions with the Nucleus, Columbia University Report, CU-175, p. 71 (1957)
17) P. A. Moldauer : *Revs. Modern Phys.*, **36**, 1079 (1964)
18) R. B. Day : "Progress in Fast Neutron Physics", The University of Chicago Press., p. 111 (1963), edited by G. C. Phillips, J. B. Marion, and J. R. Risser
19) S. M. Shafroth, P. N. Trehan, and D. M. Van Patter : *Phys. Rev.*, **129**, 704 (1963)
20) A. B. Smith, C. A. Engelbrecht, and D. Reitmann : *Phys. Rev.*, **135**, B76 (1964)